3D-Printed Kirigami-Inspired Asymmetric Dressings: Custom Elasticity and Self-Pumping for Enhanced Wound Healing

Zhen Gu[1,2], Siyang Cheng[1], Zhe Huang[1], Heng An[1], Liping Zhou[1,2], and Yongqiang Wen[1,2]

[1]Beijing Key Laboratory for Bioengineering and Sensing Technology, Daxing Research Institute, School of Chemistry & Biological Engineering, University of Science & Technology Beijing, Beijing 100083, China

[2]Author to whom correspondence should be addressed.

E-mail: guzhen@ustb.edu.cn; Liping-Zhou@ustb.edu.cn; wyq_wen@ustb.edu.cn

Supplementary figures

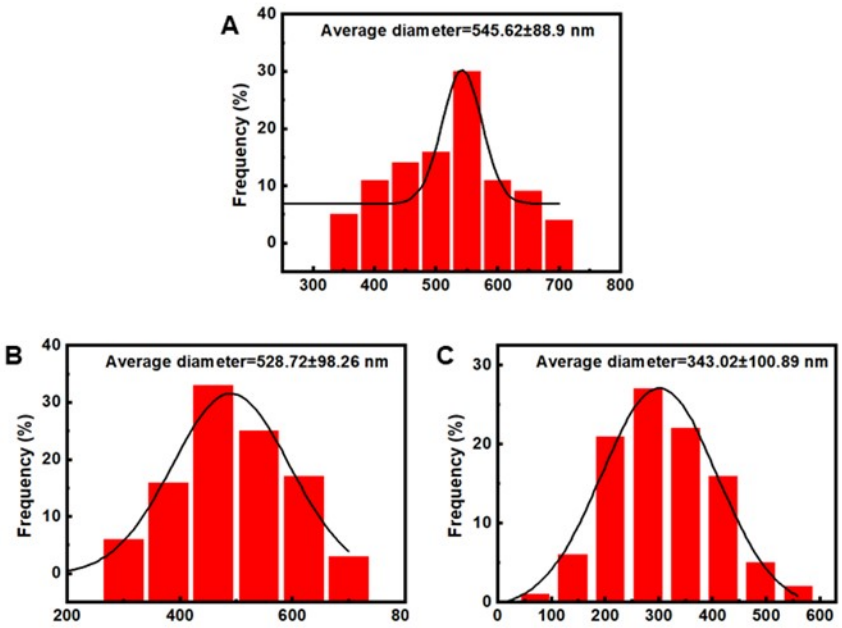

Figure S1. The diameter distribution of PU-A nanofibers at applied voltages of 20 kV (A), 25 kV (B), and 30 kV (C). The average diameters of PU-A at 20 kV, 25 kV, and 30 kV were 545.62 ± 88.9 nm, 528.72 ± 98.26 nm, and 343.02 ± 100.89 nm, respectively, exhibiting a Gaussian distribution.

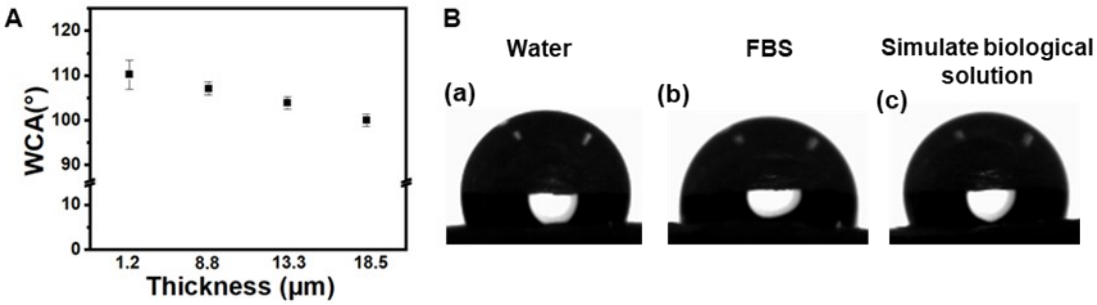

Figure S2. Characterization of PU-A Nanofibers of Varying Thicknesses in terms of wettability. (A) Effect of nanofiber thickness on contact angle. Results are presented as the mean ± standard deviation (s.d.). (n = 3). (B) Optical images of water (a), FBS (b) and simulated biological fluid (c) on hydrophobic PU-A-1.2 nanofibers (thickness of 1.2 mm). The FBS and simulated biofluid demonstrated comparable surface wetting and penetration properties with water on the hydrophobic nanofiber.

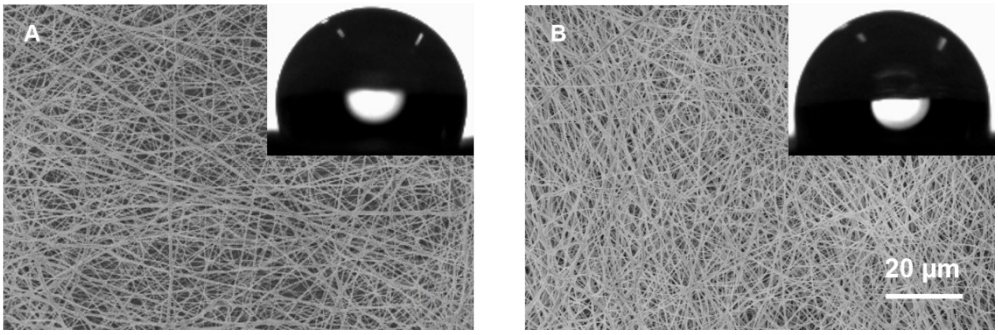

Figure S3. SEM images of hydrophobic PU (A) and PU-A nanofibers (B). The inserted images depict the optical representations of the corresponding water droplets. The addition of AgNPs does not alter the morphology or hydrophobic properties of the nanofibers.

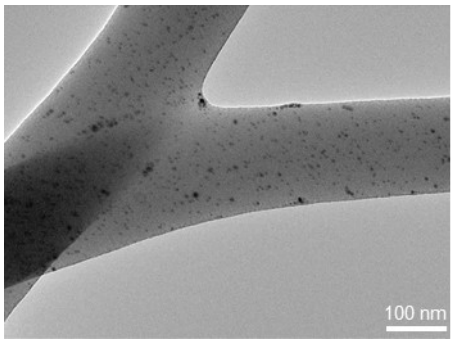

Figure S4. Transmission Electron Microscopy (TEM) images of hydrophobic and PU-A nanofibers. AgNPs were uniformly distributed on the fiber filaments, exhibiting a particle diameter of 13.5 ± 2.4 nm.

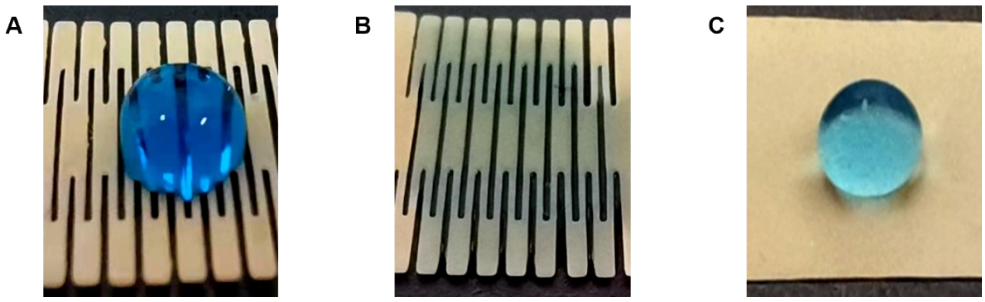

Figure S5. The optical wettability of PU-A, P3D, and PH3D was investigated. The wetting behaviors of (A) P3D before hydrophilic treatment, (B) P3D after hydrophilic treatment (PH3D), and (C) PU-A fiber membranes were investigated.

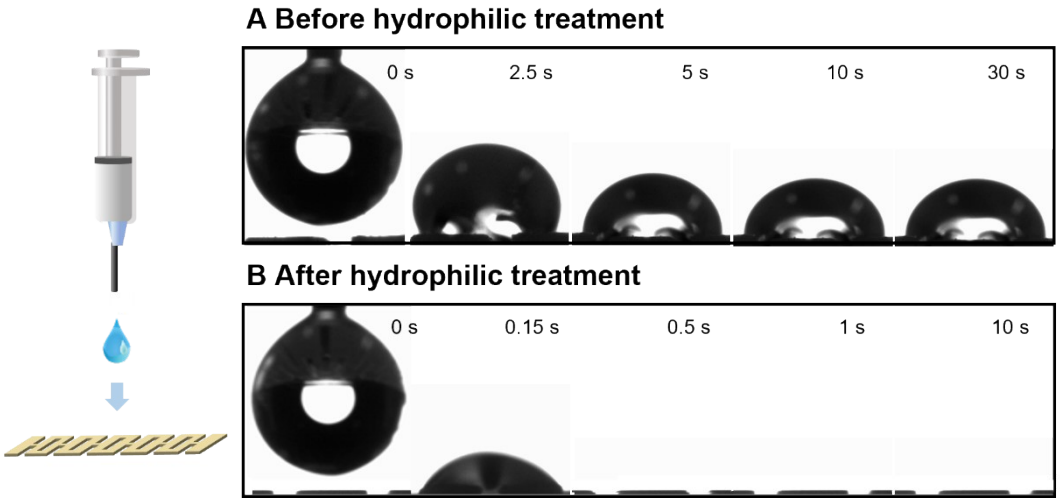

Figure S6. The dynamic diffusion behavior of droplets on (A) the P3D before hydrophilic treatment and (B) the P3D after hydrophilic treatment (PH3D) is illustrated. The contact angle of the liquid droplets on the P3D surface remained constant over a duration of 5 to 30 s. While on the PH3D surface, the liquid was fully spread out at 0.5 s.

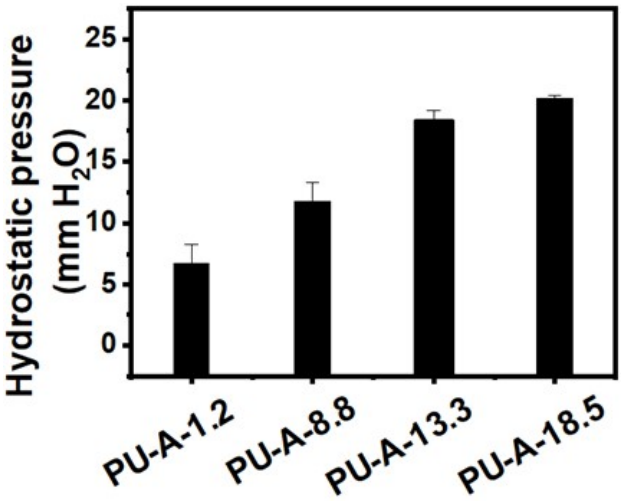

Figure S7. Hydrostatic pressure of PU-A nanofibers of different thicknesses. As the thickness of the PU-A nanofiber increases, the corresponding hydrostatic pressure also gradually rises.

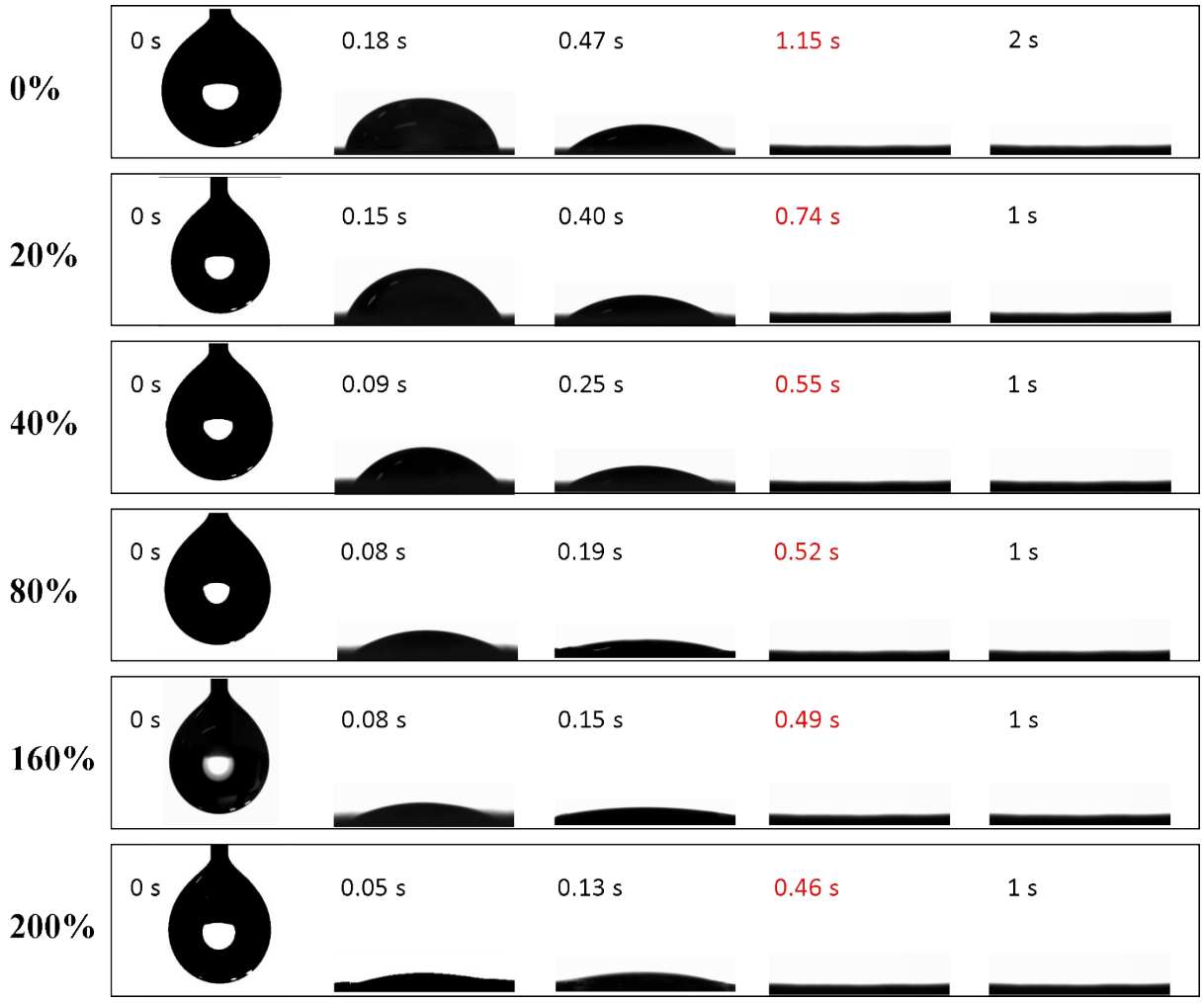

Figure S8. Dynamic evolution of water contact angle (WCA) for LD@PU-A double-layer self-pumped dressings at various elongation ratios.

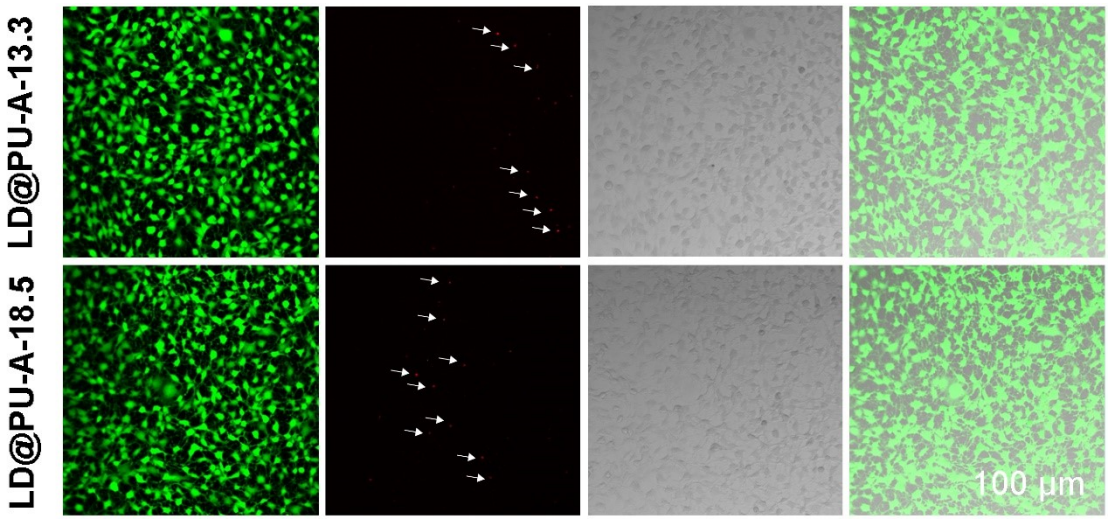

Figure S9. Representative fluorescence staining images of NIH 3T3 cells treated with LD@PU-A-13.3 and LD@PU-A-18.5. White arrows indicate dead cells.

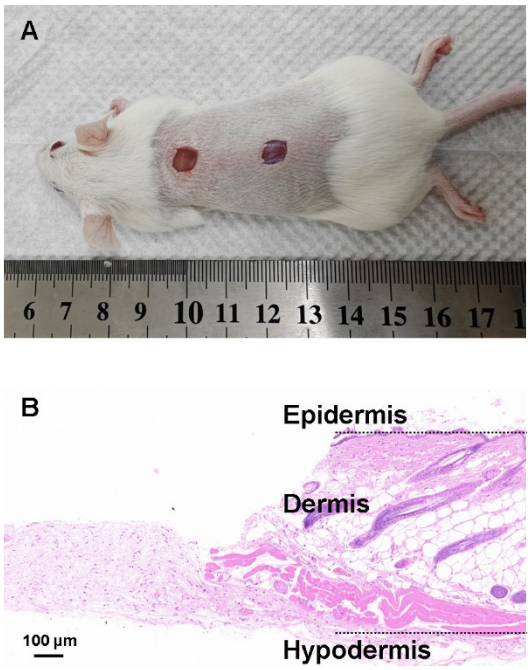

Figure S10. Representative dorsal deep wound model in mice and histological analysis of tissue damage. (A) Dorsal view of the deep-wound model in mice. (B) HE staining revealing tissue damage in deep wounds, including disruption of the epidermal and dermal layers.

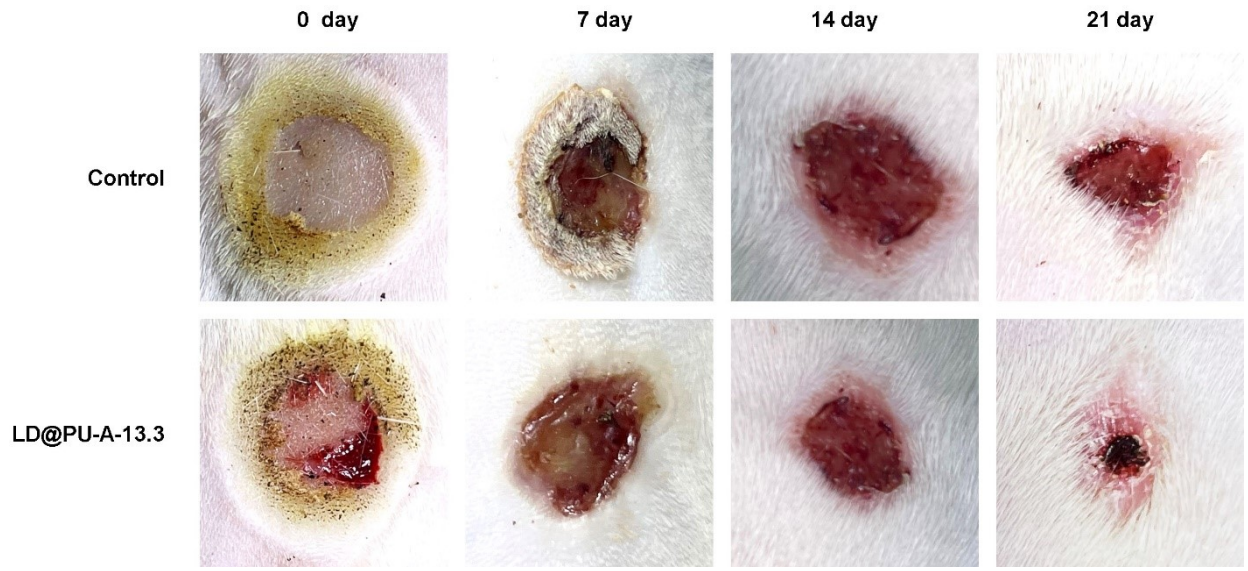

Figure S11. Burn wound healing images under control condition and LD@PU-A-13.3 nanofiber dressing treatment at 0, 7, 14, and 21 days.

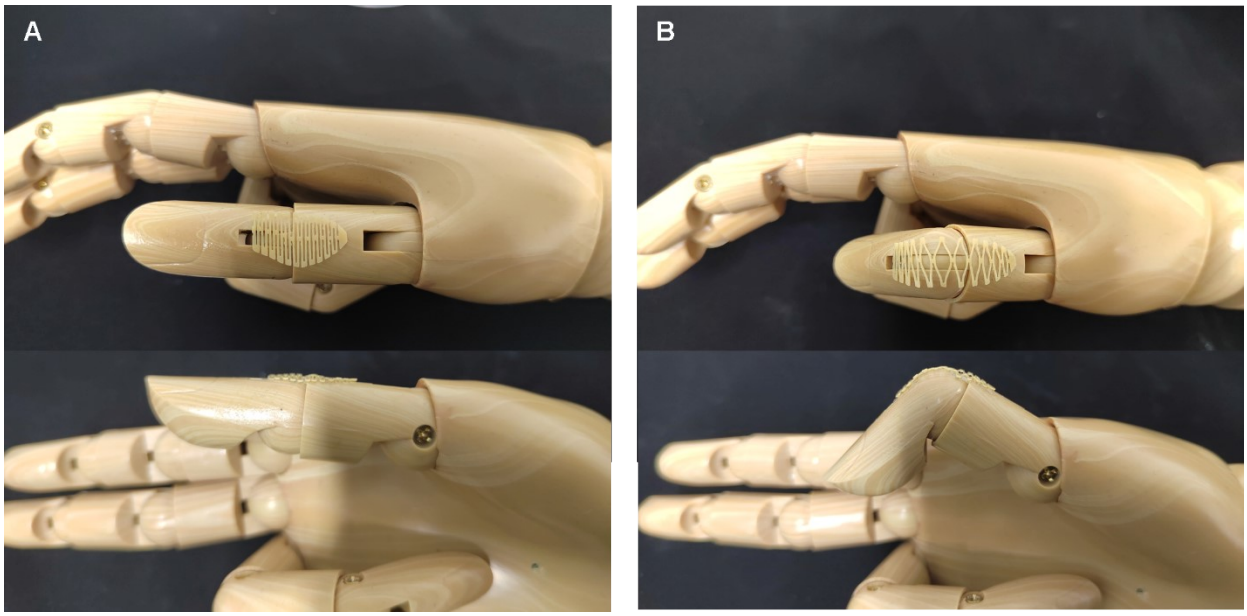

Figure S12. Photos of the LD@PU-A bilayer self-pumping dressing applied to a model joint, showing both top (upper panels) and front (lower panels) views before (A) and after (B) joint flexion.

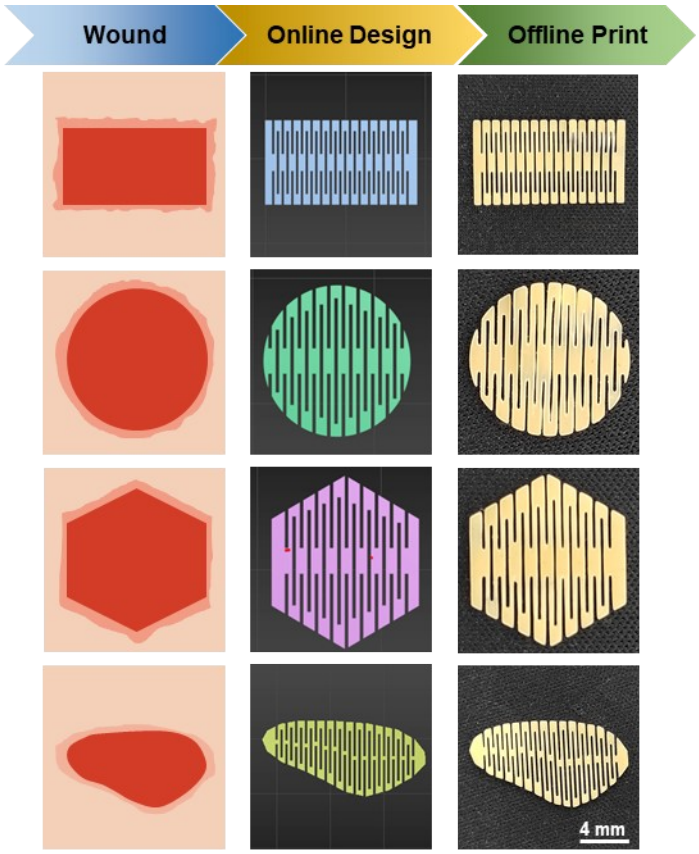

Figure S13. The personalized design of dressing shapes and the customization of precise dressing models were accomplished through accurate modeling using offline software, specifically 3D Max 2016. The dressing structure was printed to precisely conform to the shape and size of the wound. Scale: 4 mm.

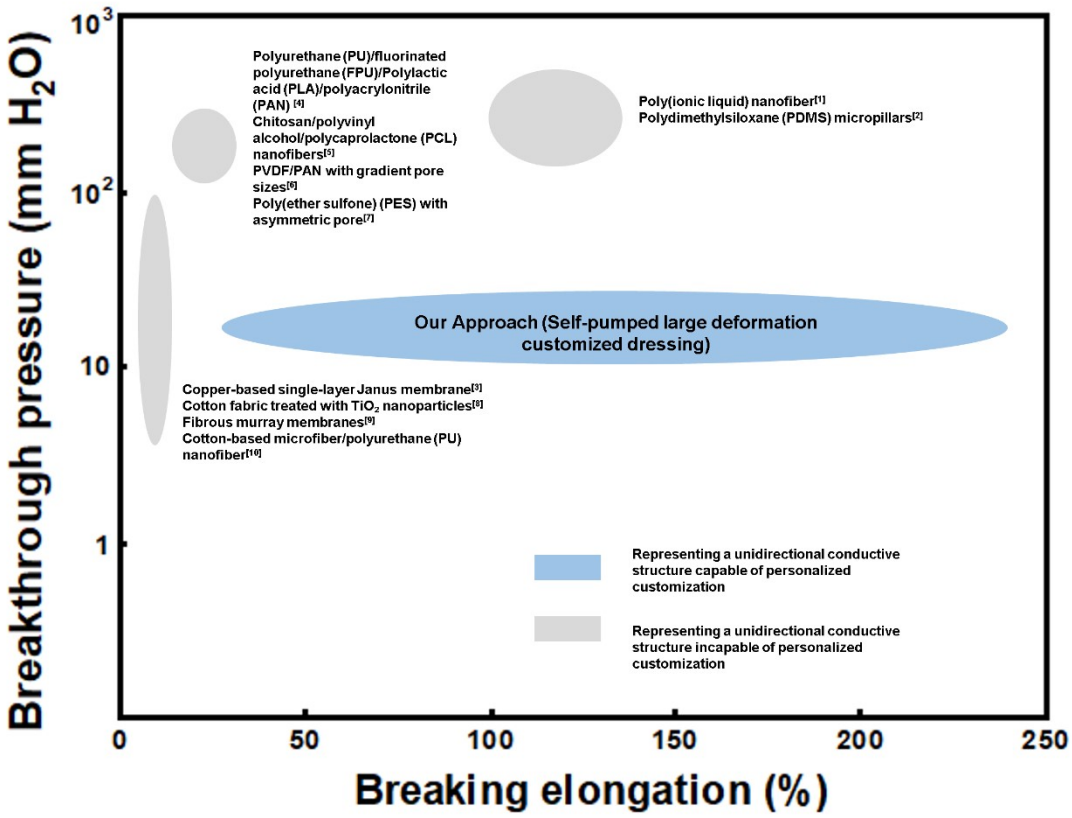

Figure S14. Performance comparison of composite membrane with unidirectional transport of tissue fluid. Under the condition that the breakthrough pressure (measured in mm H_2O) meets the actual critical requirements, the elongation of self-pumping, large-deformation custom dressings (ranging from 26% to 244%) is much wider than that reported in the literature.

Supplementary movies

Movie S1. The dynamic drainage process of the green FBS solution on the self-pumping dressing shows droplets initially contacting the hydrophobic surface and eventually being expelled through the hydrophilic end, demonstrating the ability to pass through the double-layer dressing.

Movie S2. The dynamic drainage process of the green FBS solution on the self-pumping dressing reveals droplets emerging from the lower hydrophobic end and moving toward the upper hydrophilic end, ultimately demonstrating their capacity to pass through the double-layer dressing.

Movie S3. The dynamic drainage process of the green FBS solution on the self-pumping dressing demonstrates droplets dripping from above, initially contacting the hydrophilic surface and ultimately being intercepted by fibers at the hydrophobic end, indicating that they are unable to pass through the double-layer dressing.

References

[1] S. J. Zheng; W. Z. Li; Y. Y. Ren; Z. Y. Liu; X. Y. Zou; Y. Hu; J. N. Guo; Z. Sun; F. Yan, *Adv. Mater.* **2022,** *34*, 2106570.

[2] B. B. Zhang; J. Y. Li; J. K. Zhou; L. Chow; G. Y. Zhao; Y. Huang; Z. Q. Ma; Q. Zhang; Y. W. Yang; C. K. Yiu; J. Li; F. Chun; X. C. Huang; Y. Y. Gao; P. C. Wu; S. X. Jia; H. Li; D. F. Li; Y. M. Liu; K. M. Yao; R. Shi; Z. L. Chen; B. L. Khoo; W. Q. Yang; F. Wang; Z. J. Zheng; Z. K. Wang; X. E. Yu, *Nature* **2024**, 84-92.

[3] Z. H. Zhao; Y. Z. Ning; S. Ben; X. D. Zhang; Q. Li; C. M. Yu; X. Jin; K. S. Liu; L. Jiang, *Adv. Sci.* **2022,** *9*, 2103765.

[4] Y. Y. Lin; C. Wang; D. Y. Miao; N. B. Cheng; N. Meng; A. A. Babar; X. F. Wang; B. Ding; J. Y. Yu, *ACS Appl. Mater. Interfaces* **2022,** *14*, 18944-18953.

[5] K. X. Zhang; X. Y. Jiao; L. P. Zhou; J. Wang; C. Wang; Y. Qin; Y. Q. Wen, *Biomaterials* **2021,** *276*, 121040.

[6] L. L. Yan; X. B. Yang; Y. Q. Zhang; Y. D. Wu; Z. J. Cheng; S. B. Darling; L. Shao, *Mater. Today* **2021,** *51*, 626-647.

[7] Q. Y. Zhang; Y. Li; Y. F. Yan; X. F. Zhang; D. L. Tian; L. Jiang, *ACS Nano* **2020,** *14*, 7287-7296.

[8] L. Lao; D. Shou; Y. S. Wu; J. T. Fan, *Sci. Adv.* **2020,** *6*, eaaz0013.

[9] X. F. Wang; Z. Huang; D. Y. Miao; J. Zhao; J. Y. Yu; B. Ding, *ACS Nano* **2019,** *13*, 1060-1070.

[10] L. X. Shi; X. Liu; W. S. Wang; L. Jiang; S. T. Wang, *Adv. Mater.* **2019,** *31*, 1804187